Talanta 296 (2026) 128461

Contents lists available at ScienceDirect

Talanta

journal homepage: www.elsevier.com/locate/talanta

# Photo-potentiometry: Sensing of sugars using a pH-probe coated with a film of intrinsically microporous polyamine containing graphitic carbon nitride photocatalyst

Fernanda C.O.L. Martins [a,b], Wanessa R. Melchert [c], Mariolino Carta [d], Neil B. McKeown [e], Frank Marken [a,*]

[a] Department of Chemistry, University of Bath, Claverton Down, Bath, BA2 7AY, UK
[b] Center for Nuclear Energy in Agriculture, University of São Paulo, P.O. Box 96, Piracicaba, SP, 13400-970, Brazil
[c] College of Agriculture Luiz de Queiroz, University of São Paulo, P.O. Box 9, Piracicaba, SP, 13418-970, Brazil
[d] Department of Chemistry, Swansea University, College of Science, Grove Building, Singleton Park, Swansea, SA2 8PP, UK
[e] EaStCHEM, School of Chemistry, University of Edinburgh, Joseph Black Building, David, Brewster Road, Edinburgh, EH9 3JF, Scotland, UK

ARTICLE INFO

*Keywords:*
Photo-electroanalysis
Chronopotentiometry
Photo-pH-probe
Carbohydrates
Sugary drinks

ABSTRACT

At proof-of-concept level, the photochemical transformation of glucose (or more generally of carbohydrates) can be detected analytically as a localised pH change. Using a conventional potentiometric pH-probe, a microporous coating is developed to explore carbohydrate sensing in the 200–800 μM concentration range based on localised pH changes induced by light. The photo-responsive film is based on fibrous cellulose (to aid permeability), photocatalytic graphitic carbon nitride (g-$C_3N_4$), and an intrinsically microporous polyamine host (PIM-EA-TB, as reaction environment and binder). The film-modified pH-probe is pre-conditioned in a pH 4 buffer (containing phthalate buffer). When immersed in an aqueous solution, switching on a blue LED ($\lambda = 385$ nm, approx. 60 mW $cm^{-2}$) causes a pH transient towards alkaline, which is correlated with the carbohydrate concentration (all three glucose, fructose, or sucrose give very similar signals). The LOD is typically 70 μmol $dm^{-3}$, with a linear range up to 800 μmol $dm^{-3}$. Non-linearity beyond 800 μmol $dm^{-3}$ is tentatively attributed to limited oxygen availability. The photo-electroanalytical mechanism is discussed in terms of competing proton generation and consumption in the photoactive film linked to oxygen depletion (causing alkaline drift) at the pH-probe surface.

## 1. Introduction

Glucose sensing is of global health importance due to the link between glucose level control in blood and diabetic disease or shock [1,2]. Several methods exist for glucose sensing, and in particular, electrochemical techniques have gained importance in health monitoring due to low cost and mass production opportunities. Electrochemical sensors have been embedded into wearable technology [3,4]. Apart from measurements in blood [5], there have been applications of glucose sensing in tear fluid [6], in sweat [7], in plant fluids [8], and in foods and drinks [9,10].

Most electrochemical glucose sensing mechanisms rely on anodic oxidation either by enzymes such as glucose oxidases [11], by electrocatalysis [12], or (more recently) by photo-electrocatalysis [13]. Field effect transistor sensing devices have been developed based on localised electron transfer from glucose at the gate [14]. In contrast to oxidation of glucose with enzymes or electrocatalysts where currents are linked to the transformation of glucose to gluconic acid [15], in semiconductor photo-electrocatalysis, a light pulse is applied, which triggers the formation of holes and electrons. Locally, the holes then get quenched by glucose (or carbohydrates), resulting in a current pulse linked to the electrons that are released into the conduction band [16]. The current pulse magnitude can be correlated quantitatively to the presence of the analyte. However, rather than detecting current signals, it is possible to employ the potential signal from a sensor to detect analytes during photocatalytic reactions. Here, this is demonstrated at proof-of-concept level with potentiometry at a conventional pH-probe (in contrast to the previously employed method using Pt@g-$C_3N_4$ requiring hydrogen production and a palladium membrane [13]) modified to detect sugars such as sucrose, fructose, or glucose (Fig. 1A) in commercial soft drink.

* Corresponding author.
*E-mail address:* f.marken@bath.ac.uk (F. Marken).

https://doi.org/10.1016/j.talanta.2025.128461
Received 8 April 2025; Received in revised form 11 June 2025; Accepted 13 June 2025
Available online 18 June 2025

Photo-electroanalysis [17] can be advantageous for aqueous analytes and has been applied to nitrite or glucose, but also for biosensing of glucose [18]. A modified electrode surface is required with the photocatalyst attached or embedded. It has recently been shown that intrinsically microporous polymer materials provide good hosts for photocatalysts [19]. The molecularly rigid polymer encapsulates particles but does not block catalytic surface sites.

Intrinsically microporous polymers (PIMs) [20] are based on molecularly rigid polymer backbone structures (avoiding single bonds and rotational freedom). Intrinsically microporous polyamines have found applications as hosts in electrocatalysis [21], energy storage [22], and in membrane electrochemistry [23]. The molecular structure of PIM-EA-TB [24] is shown in Fig. 1B. The Tröger base (TB) amine in the polymer backbone with ethanoanthracene units (EA) is protonated at approx. pH 4.0 [23]. Embedded into the PIM-EA-TB photoactive graphitic carbon nitride (g-$C_3N_4$ [25]) is employed here as a photoactive catalyst for the oxidation of glucose (equation (1)) in conjunction with the reduction of oxygen to hydrogen peroxide [26,27] (equation (2)).

$$\text{glucose} \rightleftarrows \text{gluconic acid} + 2\,H^+ + 2\,e^- \quad (1)$$

$$O_2 + 2\,H^+ + 2\,e^- \rightleftarrows H_2O_2 \quad (2)$$

A conventional pH-probe based on a glass membrane (Fig. 1C) would not be able to detect the presence of glucose (or carbohydrates), and processes in equations (1) and (2) are not expected to result in pH changes. However, pH gradients can be generated in films of photocatalysts when depletion of reagents occurs. Here, g-$C_3N_4$ photocatalyst is embedded into PIM-EA-TB as a microporous host. Together with fibrous cellulose, a film is applied directly to the pH-probe surface (onto the glass membrane; see Fig. 1D).

The film-modified pH-probe is investigated in aqueous media under conditions relevant to commercial soft drink analysis in the industry. Pre-conditioning and time-dependent sensing phenomena are studied. It is demonstrated that the photo-response of the sensor is insensitive to the type of carbohydrate, with glucose, fructose, and sucrose all giving essentially identical signals. All three saccharides are photo-oxidised with g-$C_3N_4$.

## 2. Experimental

### 2.1. Reagents

All solutions employed in this work were carried out using the reagents (which were glucose CAS 50-99-7, sucrose CAS 57-50-1, fructose CAS 57-48-7, potassium hydrogen phthalate CAS 877-24-7, and melamine CAS 108-78-1) from Sigma-Aldrich and purified water (18.2 MΩ cm at 20 °C). The phthalate buffer at pH 4.0, phosphate buffer at pH 7.0, and carbonate buffer at pH 10.0 were employed (Thermo Scientific Orion). PIM-EA-TB was synthesized according to a literature procedure [24]. The photocatalyst g-$C_3N_4$ was synthesized using 5 g of melamine within a ceramic boat with a lid, which was placed into a tube furnace with a temperature ramp to 500 °C, where the temperature was kept for 4 h [28].

### 2.2. Instrumentation

Chronopotentiometric analyses were performed with a potentiostat/galvanostat from Metrohm-Eco Chemie model μAUTOLB III with NOVA 2.1.2. software (Metrohm-Eco Chemie, NL). Zero current potentiometry was performed *versus* a saturated calomel electrode (SCE). Fourier transform infrared spectra (FTIR) were obtained with a Nicolet iS5 iD7ATR (Thermo Scientific, UK). A commercial glass membrane pH-probe (Voltcraft 127752) was employed. A water purification system from CE Instruments Ltd. Was used to obtain purified water with resistivity not lower than 18.2 Ωcm at 20 °C.

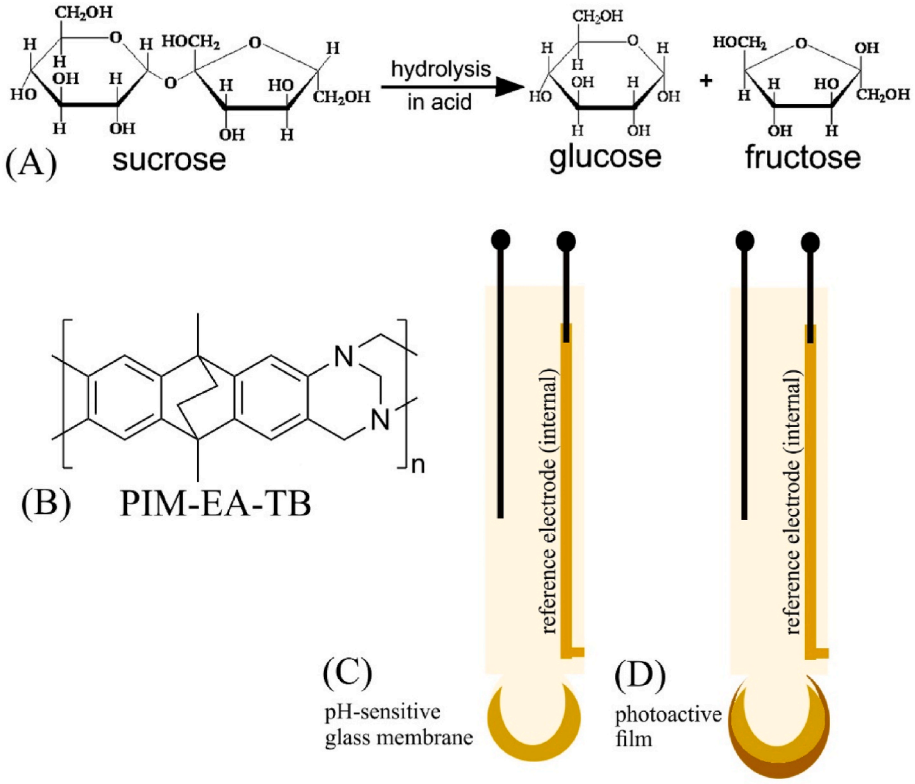


**Fig. 1.** (A) Molecular structure of sucrose and hydrolysis products glucose and fructose. (B) Molecular structure of PIM-EA-TB. Schematic showing (C) a conventional pH-probe with a glass membrane and an internal reference electrode and (D) a pH-probe with photoactive coating to allow measurement of photo-induced pH changes.

### 2.3. Procedures

**Optimization of pH-probe modification**. An analytical filter paper (Whatman no. 1) was placed in a blender and turned into a fine fibrous powder (Fig. 2A). A volume of 1 $cm^3$ of chloroform was added to the powdered paper (10 mg), then PIM-EA-TB (1 mg) and g-$C_3N_4$ (5 mg) were added, and the mixture was sonicated for 15 min. After this, the powdered paper and mixture were applied to the pH-probe surface in small drops. This immobilised the g-$C_3N_4$ with PIM-EA-TB (Fig. 2).

In FTIR data (Fig. 3) bands typical for cellulose are observed [29] in combination with those for PIM-EA-TB [30] and those for g-$C_3N_4$ [31]. In the composite, the spectral transmittance lines for cellulose and g-$C_3N_4$ dominate, but spectral features around 2850 $cm^{-1}$ are associated with PIM-EA-TB.

**Analytical parameters.** After experimental and chronopotentiometry optimization (1 data point per second over 700 s), the analytical curves were recorded in triplicate using solutions with different concentrations of glucose from 200 to 800 μmol $dm^{-3}$. The detection (LOD) and quantification limit (LOQ) were obtained employing the standard deviation (s) of the 11 measures of change in potential away from 0.23 V vs. SCE of the water and slope of the straight line of the average analytical curve based on IUPAC recommendations [32]. The repeatability (*intra-day* precision) and reproducibility (*inter-day* precision) were evaluated using a 500 μmol $dm^{-3}$ glucose solution in water. The repeatability experiments were made by measurement of 11 glucose solutions on the same day. The reproducibility experiments were carried out by the measurement of 5 different glucose solutions on different days. Subsequently, the relative standard deviations (RSD) of reproducibility and repeatability were calculated using the standard deviation of the potential difference value obtained [33].

**Application of the methodology.** The proposed methodology was applied in glucose/fructose determination in commercial soft drink samples obtained from a supermarket (Bath, UK). The samples of soft drinks (Coca Cola and Coca Cola Zero) were decarbonated by venting over three days without any additional treatment steps.

## 3. Results and discussion

### 3.1. Cellulose/g-$C_3N_4$/PIM-EA-TB coating optimization for pH-probes

Recent research has demonstrated the indirect glucose/carbohydrate determination using the g-$C_3N_4$ photocatalyst by determining liberated hydrogen (*via* a palladium membrane; employing chronopotentiometry) produced during glucose oxidation [13]. Here, a modified glass membrane is employed (without the need for hydrogen generation), and the pH-signal is monitored by chronopotentiometry.

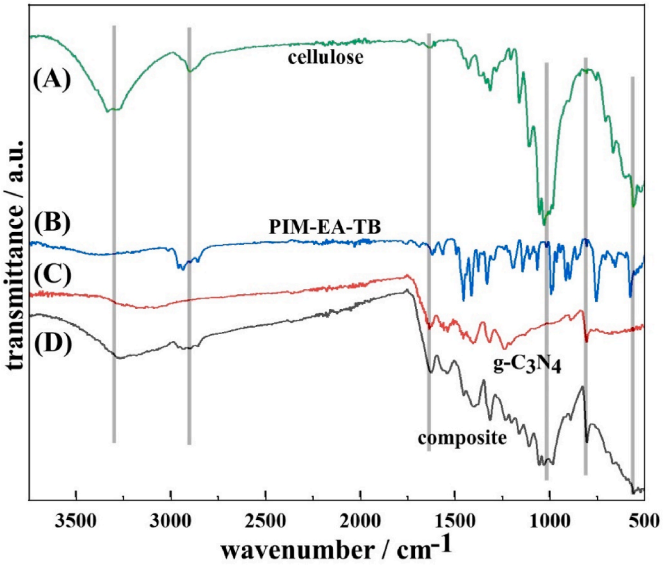


**Fig. 3.** FTIR data for (A) pure cellulose, (B) PIM-EA-TB, (C) g-$C_3N_4$, and (D) the composite applied to the pH-probe.

PIM-EA-TB is present at the pH-probe surface (i) to host the g-$C_3N_4$ photocatalyst and (ii) in order to enable mechanical stability and to fix fibrous filter paper into place. The amount of PIM-EA-TB employed was varied from 0.1 mg to 10 mg. High concentrations of PIM-EA-TB increased viscosity and caused processability problems. Low concentrations of PIM-EA-TB resulted in films peeling off and mechanical instability. Hence, 1.0 mg of PIM-EA-TB (with 10 mg cellulose and 5 mg g-$C_3N_4$) was chosen for the experiments.

Initially, test experiments were performed to evaluate the response of the modified pH-probe in the absence of light. The voltage response (vs. SCE) of the pH-probe at pH 4, 7, and 10 is plotted in Fig. 4A, consistent with a Nernstian (59 mV) shift with pH. A bare pH-probe will give a reliable pH reading within typically 60 s. In contrast, a freshly prepared modified pH-probe immersed in buffer solution will adjust very slowly due to the slow ingress of buffer and molecular species. Fig. 4B shows that a stable reading is observed in approximately 1–2 h in a pH 4 buffer. However, in pH 7 and 10 buffer solution readings, only converge toward the expected potential values after 12 h. Therefore, a pre-equilibration in pH 4 buffer solution was employed (in pH 4 phthalate buffer) with photo-pH transient experiments performed in

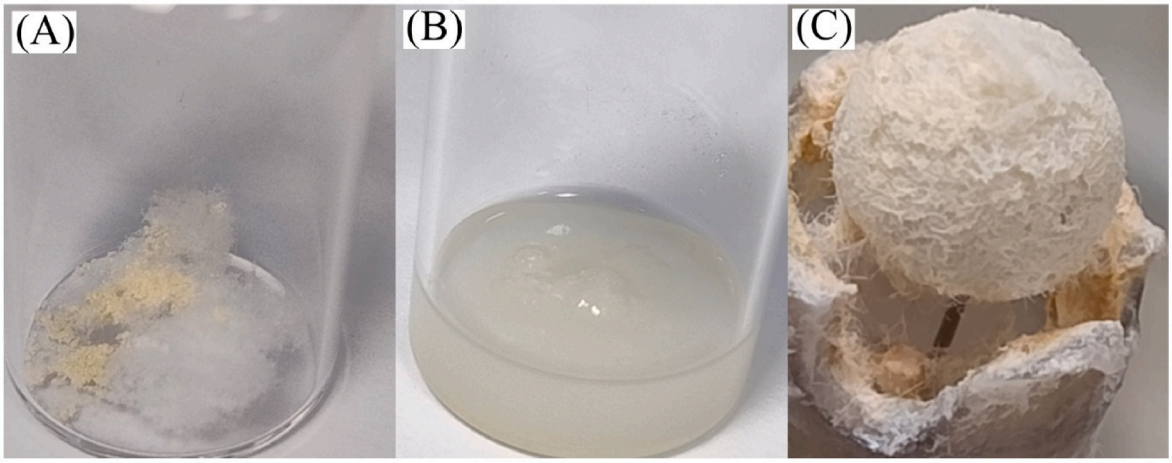


**Fig. 2.** (A) Photograph of cellulose powder with PIM-EA-TB and with g-$C_3N_4$ before dispersal. (B) Dispersed by sonication in chloroform. (C) The film (cellulose powder with PIM-EA-TB and with g-$C_3N_4$) applied to a pH-probe surface.

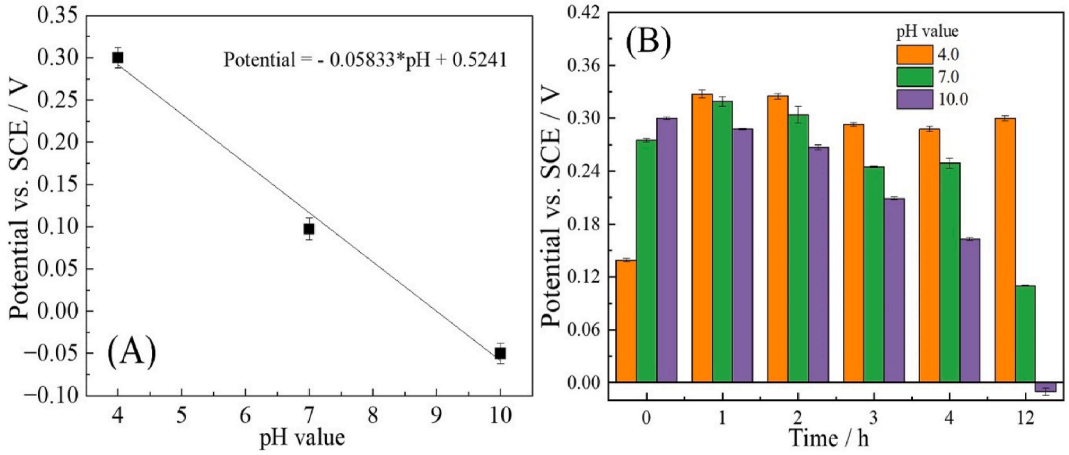


**Fig. 4.** (A) Plot of potential *versus* pH for the bare pH-probe in calibration buffer solution (Nernstian slope approx. 59 mV/pH). (B) Potential of the modified pH-probe *versus* time for three calibration buffer solutions. Equilibration is very slow, and therefore, measurements depend on the pre-equilibration conditions. Errors based on triplicate measurements.

pure unbuffered aqueous samples. These measurements are non-equilibrium measurements where pH gradients develop depending on the reaction conditions (concentration of carbohydrate, light intensity, *etc*.).

### 3.2. Glucose sensing with cellulose/g-$C_3N_4$/PIM-EA-TB-coated pH-probes

Data in Fig. 5A show pH-probe responses when transferred from a pH 4 buffer into pure water (blank) or solutions with 200 or 400 μmol $dm^{-3}$ glucose. After a period of 100 s initial drift, the LED light (λ = 385 nm, approx. 60 mW $cm^{-2}$) is switched on (typically at 0.22–0.23 V vs. SCE). With the light switched on for 600 s, a drift indicative of more alkaline conditions (lower potential) is observed. The presence of glucose increases the apparent pH drift. This experiment works well when the pH-probe is pre-equilibrated in pH 4 phthalate buffer. Fig. 5B shows that experiments with pre-equilibration in pH 7 phosphate buffer were not successful. Fig. 5C demonstrates that transient signals are generated after pre-equilibration in pH 4 phosphate buffer; however, they exhibit lower reproducibility. Perhaps interestingly, both the phthalate buffer and amaranth red dye in the commercial buffer solution seem to help produce reproducible data (Fig. 5D). Fig. 5E shows data for repeated switching of the LED light with pH transients clearly being related to the light signal.

For calibration purposes, the pH-probe was modified with cellulose, g-$C_3N_4$, and PIM-EA-TB, pre-equilibrated in pH 4 buffer, and then immersed in pure water with glucose concentrations from 200 to 800 μmol $dm^{-3}$ (Fig. 6). Glucose photo-potential responses ΔE were measured 600 s after switching the LED on and in triplicate, and the chronopotentiometry data are presented in Fig. 6A. A linear correlation of the potential drift ΔE and glucose concentration is observed up to 800 μmol $dm^{-3}$ (Fig. 6B). At higher glucose levels, the data points plateau, which is tentatively attributed here to the complete depletion of oxygen in the solution (see below).

Fig. 6B presents a linear analytical curve with a correlation coefficient (r) equal to 0.99, demonstrating linearity over a limited concentration range. The LOD, LOQ, repeatability, and reproducibility were 70.1 μmol $dm^{-3}$ (12.6 mg $dm^{-3}$), 212 μmol $dm^{-3}$ (38.2 mg $dm^{-3}$), 3.95 %, and 4.43 %, respectively. Equation (3) represents the average analytical curve of glucose, along with the confidence intervals (CI) for the slope and intercept.

$$\Delta E\ (V) = 7.84x10^{-5}\left(\pm 1.76x10^{-5}\right)[Glucose]\left(\frac{Vdm^3}{mol}\right) + 2.58x10^{-2}\left(\pm 2.58x10^{-2}\right)(V) \quad (3)$$

The CI was calculated using (equation (4)).

$$CI = value\ \pm \frac{ts}{\sqrt{n}} \quad (4)$$

The statistical *t*-value was consistent with a $t_{tabulated}$ value with a confidence level of 95 %. The value was the average value of the slope and interception, with *s* the standard deviation of the slope and interception values, and *n* the determination number. This suggests that the proposed analytical procedure did not have significant systematic errors.

### 3.3. Analytical parameters for sugar sensing in a soft drink

Soft drink samples were based on commercial drinks (Coca Cola and Coke Zero, see Experimental). Initially, the recoveries of glucose were evaluated using sample volumes of 25 μL (101.10 ± 5.4 %) and 2.5 mL (99.13 ± 3.6 %) of Coke Zero, with a final volume of 25 mL, to assess the matrix effect. This demonstrated that the concomitant compounds did not interfere with the glucose determination. The sugar content of the soft drink (Coca Cola) was given as 10.6 g per 100 $cm^3$. However, the type of sugar is not well defined here. Sucrose will hydrolyse to fructose and glucose (see Fig. 1) under conditions of storage and use. Therefore, the chemical nature of the sugar needs to be considered.

The data for the analysis are presented in Fig. 7. Standard additions of 400, 500, and 600 μmol $dm^{-3}$ glucose, fructose, and sucrose were employed in a soft drink free sample. The sugar quantity based on glucose calculated for the sugar-containing soft drink sample was determined to be equivalent to 11.5 ± 0.7 g glucose per 100 $cm^3$, which compared well to the value presented on the label (10.6 g per 100 $cm^3$). This suggests that most of the sucrose is hydrolysed and present as glucose/fructose (Fig. 1; *vide infra*).

The significance of the "*t*-test" was calculated based on equation (5) due to the evaluation of the accuracy of the proposed methodology.

$$t = (\overline{x} - \mu)\ \pm \frac{\sqrt{n}}{s} \quad (5)$$

Here, *n* is the experiment repetitions number, *s* is the interception standard deviation, $\mu$ is the value expected (10.6 g per 100 $cm^3$), and $\overline{x}$ is the average obtained concentration of sugar. The $|t|$ calculated was 2.21, which presented a value lower than the critical value tabulated ($t_{critical}$ = 4.30) at a confidence level of 95 %, confirming that there are no significant differences between the value obtained in this method and the packaging value. However, the reactivity of different sugars needs to be considered.

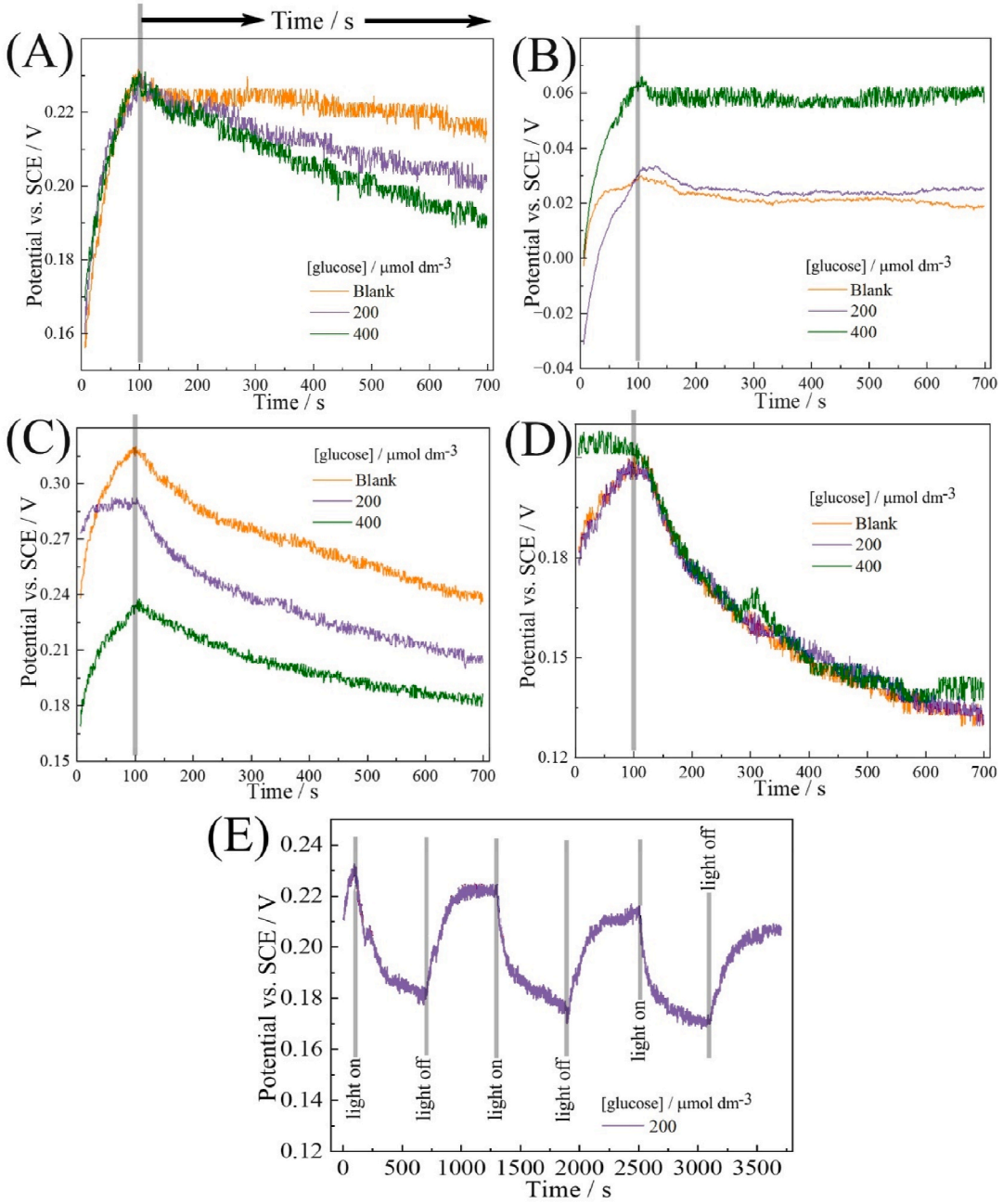


**Fig. 5.** Chronopotentiometry (zero current) for glucose detection employing a pH-probe modified with 10 mg of cellulose powder, 5 mg g-$C_3N_4$, and 1 mg PIM-EA-TB immersed in pure water, and 0, 200, and 400 µmol $dm^{-3}$ glucose dissolved. Light-on for LED ($\lambda$ = 385 nm, approx. 60 mW $cm^{-2}$) indicated by a grey line. (A) Pre-equilibrated in phthalate buffer solution at pH 4.0 with amaranth red dye. (B) Pre-equilibrated in phosphate buffer solution at pH 7.0. (C) Pre-equilibrated in phosphate buffer at pH 4.0 with amaranth red dye. (D) Pre-equilibrated in phthalate buffer at pH 4.0 without amaranth red dye. (E) Signal for multiple light pulses.

In order to explore the responses to glucose, fructose, and sucrose, addition-recovery experiments were performed with standard additions of 400, 500, and 600 µmol $dm^{-3}$ glucose, fructose, and sucrose in the soft drink zero sample. Table 1 summarises the data, showing that all three sugars yield recoveries of close to 100 %. Without the hydrolysis of the sucrose, the expected sensor response would have been only half of the observed response. Table 2 compares the new photopotentiometry method with other known literature methods for sugar detection.

By employing commercial soft drink samples with carbohydrate content dominated by sugars, the question of interfering species is not clearly addressed. The detection of sucrose, fructose, and glucose results in very similar analytical signals and other similar molecules could give similar signals. It has been reported in the literature that non-reducing sugars or relatively inert molecules such as sorbitol under similar conditions are effectively photo-oxidised by g-$C_3N_4$ [39]. Therefore, for analysis in more complex sample matrices (*e.g.* milk), selectivity to specific analytes will require further attention/study. Improved selectivity towards an analyte and suppression of interfering species could be possible in future by varying the host polymer nature or by tuning down/changing the photocatalyst.

### 3.4. Hypothetical mechanism

Although photo-electroanalytical tools for glucose/carbohydrate detection are well-established, there is no previous detection with a surface-modified pH-probe. Glass membrane pH-probes are readily

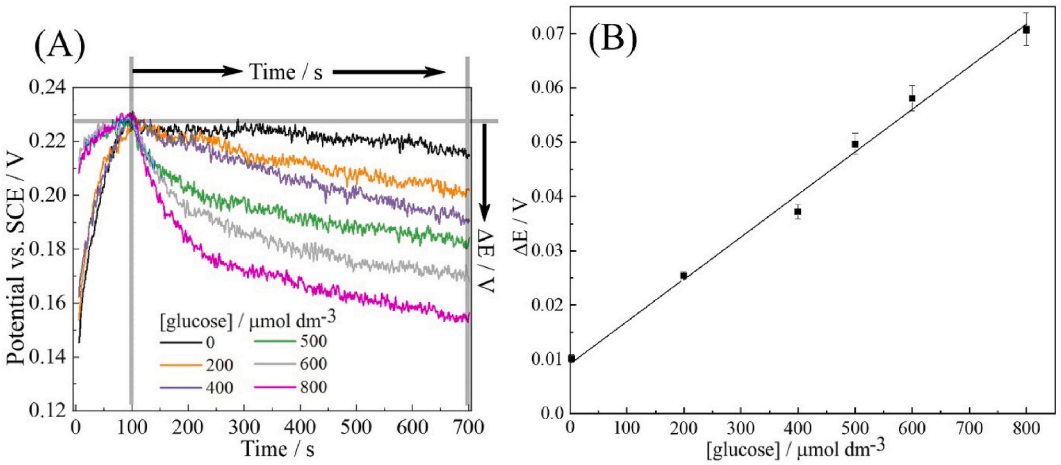


**Fig. 6.** (A) Chronopotentiometry (zero current) for glucose detection employing a pH-probe modified with 10 mg of cellulose powder, 5 mg g-$C_3N_4$, and 1 mg PIM-EA-TB (pre-equilibrated in pH 4 buffer) in pure water in concentration intervals from 200 to 800 μmol $dm^{-3}$. (B) Relationship between the difference potential and glucose concentration (repeats n = 3).

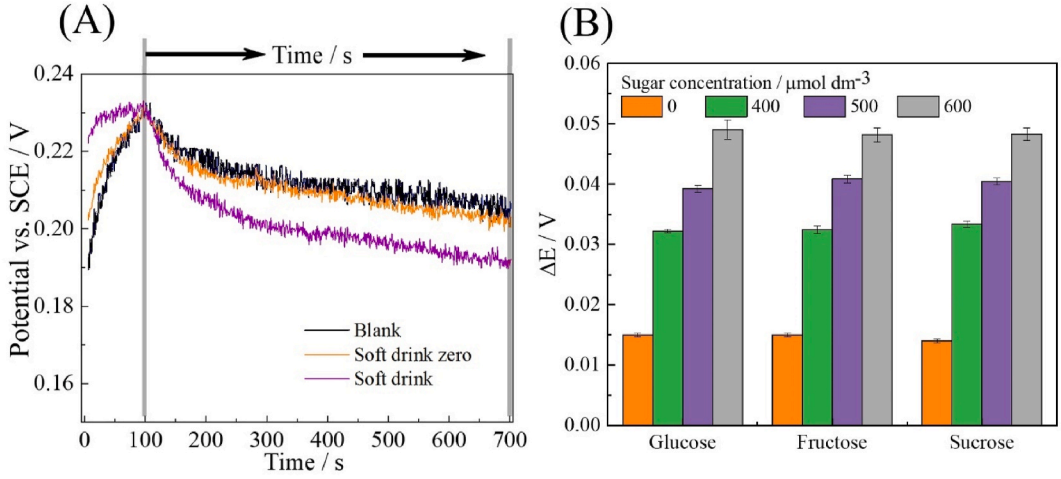


**Fig. 7.** (A) Chronopotentiometry (zero current) for glucose detection employing a pH-probe modified with 10 mg of cellulose powder, 5 mg g-$C_3N_4$, and 1 mg PIM-EA-TB (equilibrated in pH 4 buffer) in 25 mL pure water without and with the addition of 21 μL of soft drink zero and soft drink. (B) Photo-potential responses for glucose, fructose and sucrose solutions detection employing a pH-probe modified with 10 mg of cellulose, 5 mg g-$C_3N_4$, and 1 mg PIM-EA-TB in pure water, and 0, 200, and 400 μmol $dm^{-3}$ glucose, fructose, and sucrose solutions.

**Table 1**
Addition-recovery for different sugars employing pH-probe modified with 10 mg cellulose powder, 5 mg g-$C_3N_4$, and 1 mg PIM-EA-TB (pre-equilibration in phthalate buffer at pH 4) in soft drink free of sugar (n = 3).

| Added concentration (μmol $dm^{-3}$) | Recoveries (%) | | |
|---|---|---|---|
| | Glucose | Fructose | Sucrose |
| 400 | 98.0 ± 0.9 | 98.9 ± 3.0 | 101.8 ± 1.8 |
| 500 | 96.8 ± 1.5 | 101.1 ± 1.6 | 100.0 ± 1.5 |
| 600 | 102.1 ± 2.6 | 101.2 ± 3.5 | 100.5 ± 2.3 |

available and used for standard analysis. The modification of this kind of analytical probe with a photo-active film to detect specific analytes could have wider applications.

When considering the mechanism of carbohydrate detection, photochemical processes within the film have to be considered. It has been previously shown that photo-driven oxidation of carbohydrates occurs at g-$C_3N_4$ modified surfaces [13]. Fig. 8 summarises typical processes, such as the 2-electron oxidation of an alcohol to an aldehyde and the 2-electron oxidation of an aldehyde to a carboxylic acid. To balance the consumption of photo-generated holes and electrons, these processes must be coupled to the reduction of oxygen, leading to the production of $H_2O_2$ under these conditions [26]. All of these processes appear to be overall redox-neutral and pH-neutral, but the consumption of oxygen will lead to a gradient with less and less oxygen closer to the glass membrane. The associated more reducing conditions can trigger additional processes such as the reduction/consumption of protons, which causes a drift in pH toward more alkaline conditions at the glass membrane surface. The depletion of oxygen is likely a key part of the mechanism, which can explain the analytical range being limited to below 1 mM glucose (see Fig. 8).

The mechanism is not selective as g-$C_3N_4$ is reactive towards many types of carbohydrates, including non-reducing sugars or sorbitol [27]. In the case of sugar analysis in soft drinks, this non-selectivity is beneficial by reporting the total sugar concentration. In the future, the photo-active film could be designed/modified to provide higher sensitivity (*e.g.* limiting oxygen depletion) or higher selectivity (*e.g.* employing more selective photocatalysts).

**Table 2**
Some analytical parameters for the determination methods for sugars.

| Method[a] | Working range/mg $dm^{-3}$ | Analysis time/ min | LOD/mg $dm^{-3}$ | Sample preparation[a] | Ref. |
|---|---|---|---|---|---|
| Colorimetric | 400–1000 | 10 | 360 | LLE | [34] |
| HILIC-MS/MS | 0.0000202–0.057 | 25 | 0.0012–0.228 | UAE extraction | [35] |
| HPLC-ELSD | 4.00–400 | 50 | 8.00–40.00 | SPE extraction | [36] |
| CuNP-ink/PDEs and CV | 0.22–7.21 | 0.025 | 0.090 | Filtered and diluted with 0.1 M NaOH solution | [37] |
| CCM/GCE-modified and chronoamperometry | 0.11–45.04 | 1.66 | 0.047 | Extraction using electrostatic repulsion and adsorption | [38] |
| Pt@g-$C_3N_4$ and chronopotentiometry | 1801–180156 | 16.67 | – | Filtration and dilution with water | [13] |
| Photo-potentiometric | 36.03–144.12 | 11.66 | 12.60 mg $dm^{-3}$ | Dilution with water | This work |

[a] CCM/GCE = Cu/$Cu_2O$@MOF(Cu)/glassy carbon electrode; CV = Cyclic voltammetry; ELSD = evaporative light-scattering detector; HILIC = hydrophilic interaction chromatography; LLE = liquid-liquid extraction; MS/MS = electrospray ionization-tandem mass spectrometry; PDEs = pencil-drawn electrodes; SPE = solid-phase extraction; UAE = ultrasonic-assisted extraction.

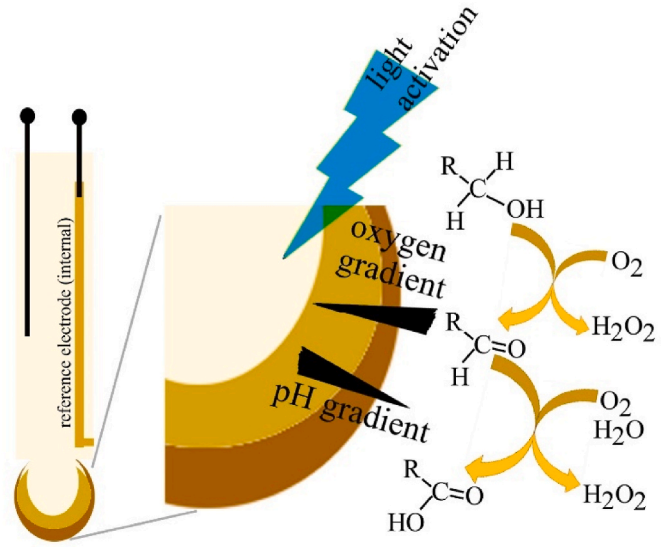


**Fig. 8.** Schematic of the hypothetical mechanism based on oxygen depletion and more reducing conditions close to the glass membrane when light is applied.

## 4. Conclusions

It has been shown at proof-of-concept level that the photo-potentiometric sensing of glucose/carbohydrates is possible with modified glass membrane pH-probes. A film composite containing cellulose (10 mg), g-$C_3N_4$ (5 mg), and PIM-EA-TB (1 mg) was pre-equilibrated in pH 4 phthalate buffer (containing amaranth red dye) and then transferred into the measurement solution. The polymer of intrinsic microporosity provides an active embedded photocatalyst without blocking photocatalytic sites. Switching on a blue LED ($\lambda = 385$ nm; 60 mW $cm^{-2}$) caused a potential drift towards alkaline pH caused by glucose-driven photochemical processes in the microporous film. With a 600 s measurement time a good correlation of the pH-drift (expressed as $\Delta E$) and carbohydrate concentration was observed. The mechanism has been tentatively assigned to oxygen depletion coupled with pH-drift.

The practical significance of this new methodology is in the simplicity of combining a potentiometric measurement tool with a widely available pH glass-probe and without the need for hydrogen generation. In the future, low-cost sensing based on commercial pH-probes will be possible for a wider range of analytes, as long as photo-active films with selectivity and reactivity can be identified and applied to the pH sensor. In the future, selectivity towards analytes and suppression of signals due to interfering species could be improved by varying the host polymer and/or by modification of the photocatalyst. Other types of potentiometric probes (*e.g.* sensitive to fluoride) could further broaden the application of microporous polymer-based photo-potentiometry.

## CRediT authorship contribution statement

**Fernanda C.O.L. Martins:** Writing – original draft, Methodology, Investigation, Formal analysis, Data curation. **Wanessa R. Melchert:** Writing – review & editing, Supervision, Funding acquisition, Conceptualization. **Mariolino Carta:** Writing – review & editing, Supervision, Resources, Conceptualization. **Neil B. McKeown:** Writing – review & editing, Supervision, Resources, Methodology, Conceptualization. **Frank Marken:** Writing – review & editing, Writing – original draft, Supervision, Formal analysis, Conceptualization.

## Declaration of competing interest

The authors declare that they have no known competing financial interests or personal relationships that could have appeared to influence the work reported in this paper.

## Acknowledgements

F.C.O.L. Martins and W.R. Melchert acknowledge the financial support from Brazilian Government Agencies, including the Brazilian National Council for Scientific and Technological Development (CNPq, grants 305538/2022–5) and, in part by the Coordination of Superior Level Staff Improvement (CAPES) - Finance Code 001. F. Marken acknowledges initial funding from EPSRC (EP/K004956/1).

## Data availability

Data will be made available on request.

## References

[1] J.R. Windmiller, J. Wang, Wearable electrochemical sensors and biosensors: a review, Electroanalysis 25 (2013) 29–46, https://doi.org/10.1002/elan.201200349.
[2] N.J. Ronkainen, H.B. Halsall, W.R. Heineman, Electrochemical biosensors, Chem. Soc. Rev. 39 (2010) 1747–1763, https://doi.org/10.1039/b714449k.
[3] J. Kim, A.S. Campbell, J. Wang, Wearable non-invasive epidermal glucose sensors: a review, Talanta 177 (2018) 163–170, https://doi.org/10.1016/j.talanta.2017.08.077.
[4] C. Harito, L. Utari, B.R. Putra, B. Yuliarto, S. Purwanto, S.Z.J. Zaidi, D. Bavykin, F. Marken, F.C. Walsh, Review - the development of wearable polymer-based sensors: perspectives, J. Electrochem. Soc. 167 (2020) 037566, https://doi.org/10.1149/1945-7111/ab697c.
[5] L. Tang, S.J. Chang, C.J. Chen, J.T. Liu, Non-invasive blood glucose monitoring technology: a review, Sensors 20 (2020) 6925, https://doi.org/10.3390/s20236925.
[6] N.M. Farandos, A.K. Yetisen, M.J. Monteiro, C.R. Lowe, S.H. Yun, Contact lens sensors in ocular diagnostics, Adv. Healthcare Mater. 4 (2015) 792–810, https://doi.org/10.1002/adhm.201400504.

[7] Y.R. Yang, W. Gao, Wearable and flexible electronics for continuous molecular monitoring, Chem. Soc. Rev. 48 (2019) 1465–1491, https://doi.org/10.1039/c7cs00730b.

[8] C. Diacci, T. Abedi, J.W. Lee, E.O. Gabrielsson, M. Berggren, D.T. Simon, T. Niittylä, E. Stavrinidou, Diurnal in vivo xylem sap glucose and sucrose monitoring using implantable organic electrochemical transistor sensors, iScience 24 (2021) 101966, https://doi.org/10.1016/j.isci.2020.101966.

[9] H.T. Wang, W.X. Zhu, T. Xu, Y.X. Zhang, Y.J. Tian, X. Liu, J.L. Wang, M. Ma, An integrated nanoflower-like $MoS_2$@$CuCo_2O_4$ heterostructure for boosting electrochemical glucose sensing in beverage, Food Chem. 396 (2022) 133630, https://doi.org/10.1016/j.foodchem.2022.133630.

[10] S. Cinti, R. Marrone, V. Mazzaracchio, D. Moscone, F. Arduini, Novel bio-lab-on-a-tip for electrochemical glucose sensing in commercial beverages, Biosens. Bioelectron. 165 (2020) 112334, https://doi.org/10.1016/j.bios.2020.112334.

[11] C. Chen, Q.J. Xie, D.W. Yang, H.L. Xiao, Y.C. Fu, Y.M. Tan, S.Z. Yao, Recent advances in electrochemical glucose biosensors: a review, RSC Adv. 3 (2013) 4473–4491, https://doi.org/10.1039/c2ra22351a.

[12] S. Park, H. Boo, T.D. Chung, Electrochemical non-enzymatic glucose sensors, Anal. Chim. Acta 556 (2006) 46–57, https://doi.org/10.1016/j.aca.2005.05.080.

[13] Y.Z. Zhao, J. Dobson, C. Harabajiu, E. Madrid, T. Kanyanee, C. Lyall, S. Reeksting, M. Carta, N.B. McKeown, L. Torrente-Murciano, K. Black, F. Marken, Indirect photo-electrochemical detection of carbohydrates with Pt@g-$C_3N_4$ immobilised into a polymer of intrinsic microporosity (PIM-1) and attached to a palladium hydrogen capture membrane, Bioelectrochemistry 134 (2020) 107499, https://doi.org/10.1016/j.bioelechem.2020.107499.

[14] A. Barbaro, C. Colapicchioni, E. Davini, G. Mazzamurro, A.P. Piotto, F. Porcelli, ChemFET devices for biomedical and environmental applications, Adv. Mater. 4 (1992) 402–408, https://doi.org/10.1002/adma.19920040605.

[15] P. Martinkova, M. Pohanka, Biosensing for blood glucose and diabetes diagnosis: evolution, construction, and current status, Anal. Lett. 48 (2015) 2509–2532, https://doi.org/10.1080/00032719.2015.1043661.

[16] S.F. Blaskievicz, L.H. Mascaro, Y.Z. Zhao, F. Marken, Semiconductor photoelectroanalysis and photobioelectroanalysis: a perspective, Trac. Trends Anal. Chem. 135 (2021) 116154, https://doi.org/10.1016/j.trac.2020.116154.

[17] Y.Z. Zhao, N.A. Al Abass, R. Malpass-Evans, M. Carta, N.B. McKeown, E. Madrid, P. J. Fletcher, F. Marken, Photoelectrochemistry of immobilised Pt@g-$C_3N_4$ mediated by hydrogen and enhanced by a polymer of intrinsic microporosity PIM-1, Electrochem. Commun. 103 (2019) 1–6, https://doi.org/10.1016/j.elecom.2019.04.006.

[18] W.W. Zhao, J.J. Xu, H.Y. Chen, Photoelectrochemical enzymatic biosensors, Biosens. Bioelectron. 92 (2017) 294–304, https://doi.org/10.1016/j.bios.2016.11.009.

[19] A. Karunakaran, C.R. Bowen, S. Dunn, T.P.T. Pham, A. Folli, P.J. Fletcher, M. Carta, N.B. McKeown, F. Marken, Molecularly rigid porous polyamine host enhances barium titanate catalysed H2O2 generation, New J. Chem. 48 (2024) 16261–16268, https://doi.org/10.1039/d4nj03460k.

[20] F. Marken, M. Carta, N.B. McKeown, Polymers of intrinsic microporosity in the design of electrochemical multicomponent and multiphase interfaces, Anal. Chem. 93 (2021) 1213–1220, https://doi.org/10.1021/acs.analchem.0c04554.

[21] A. Kolodziej, S.D. Ahn, M. Carta, R. Malpass-Evans, N.B. McKeown, R.S. L. Chapman, S.D. Bull, F. Marken, Electrocatalytic carbohydrate oxidation with 4-benzoyloxy-TEMPO heterogenised in a polymer of intrinsic microporosity, Electrochim. Acta 160 (2015) 195–201, https://doi.org/10.1016/j.electacta.2015.01.106.

[22] L.N. Wang, Y.Z. Zhao, B.B. Fan, M. Carta, R. Malpass-Evans, N.B. McKeown, F. Marken, Polymer of intrinsic microporosity (PIM) films and membranes in electrochemical energy storage and conversion: a mini-review, Electrochem. Commun. 118 (2020) 106798, https://doi.org/10.1016/j.elecom.2020.106798.

[23] E. Madrid, Y.Y. Rong, M. Carta, N.B. McKeown, R. Malpass-Evans, G.A. Attard, T. J. Clarke, S.H. Taylor, Y.T. Long, F. Marken, Metastable ionic diodes derived from an amine-based polymer of intrinsic microporosity, Angew. Chem. Int. Ed. 53 (2014) 10751–10754, https://doi.org/10.1002/anie.201405755.

[24] M. Carta, R. Malpass-Evans, M. Croad, Y. Rogan, J.C. Jansen, P. Bernardo, F. Bazzarelli, N.B. McKeown, An efficient polymer molecular sieve for membrane gas separations, Science 339 (2013) 303–307, https://doi.org/10.1126/science.1228032.

[25] S.W. Cao, J.X. Low, J.G. Yu, M. Jaroniec, Polymeric photocatalysts based on graphitic carbon nitride, Adv. Mater. 27 (2015) 2150–2176, https://doi.org/10.1002/adma.201500033.

[26] A. Karunakaran, K.J. Francis, C.R. Bowen, R.J. Ball, Y.Z. Zhao, L.N. Wang, N. B. McKeown, M. Carta, P.J. Fletcher, R. Castaing, M.A. Isaacs, L.J. Hardwick, G. Cabello, I.V. Sazanovich, F. Marken, Nanophase-photocatalysis: loading, storing, and release of $H_2O_2$ using graphitic carbon nitride, Chem. Commun. 59 (2023) 7423–7426, https://doi.org/10.1039/d3cc01442h.

[27] Y.Z. Zhao, L.N. Wang, R. Malpass-Evans, N.B. McKeown, M. Carta, J.P. Lowe, C. L. Lyall, R. Castaing, P.J. Fletcher, G. Kociok-Köhn, J. Wenk, Z.Y. Guo, F. Marken, Effects of g-$C_3N_4$ heterogenization into intrinsically microporous polymers on the photocatalytic generation of hydrogen peroxide, ACS Appl. Mater. Interfaces 14 (2022) 19938–19948, https://doi.org/10.1021/acsami.1c23960.

[28] A. Karunakaran, H.D.P. Nguyen, C.R. Bowen, F. Marken, B. Narayan, S. Dunn, Y. Zhang, M. Jia, Y. Zhao, N.P. Nguyen, B.N.T. Le, T.P.T. Pham, Understanding the effect of saturated gases on catalytic performance of graphitic carbon nitride (g-$C_3N_4$) for $H_2O_2$ generation and dye degradation in the presence of ultrasound, Adv. Eng. Mater. 26 (2024) 2301958, https://doi.org/10.1002/adem.202301958.

[29] V. Hospodarova, E. Singovszka, N. Stevulova, Characterization of cellulosic fibers by FTIR - spectroscopy for their further implementation to building materials, Am. J. Anal. Chem. 9 (2018) 303–310, https://doi.org/10.4236/ajac.2018.96023.

[30] R. Tan, A.Q. Wang, R. Malpass-Evans, R. Williams, E.W. Zhao, T. Liu, C.C. Ye, X. Q. Zhou, B.P. Darwich, Z.Y. Fan, L. Turcani, E. Jackson, L.J. Chen, S.M.Y. Chong, T. Li, K.E. Jelfs, A.I. Cooper, N.P. Brandon, C.P. Grey, N.B. McKeown, Q.L. Song, Hydrophilic microporous membranes for selective ion separation and flow-battery energy storage, Nat. Mater. 19 (2020) 195–197, https://doi.org/10.1038/s41563-019-0536-8.

[31] S. Pareek, M. Sharma, S. Lal, J.K. Quamara, Polymeric graphitic carbon nitride-barium titanate nanocomposites with different content ratios: a comparative investigation on dielectric and optical properties, J. Mater. Sci. Mater. Electron. 29 (2018) 13043–13051, https://doi.org/10.1007/s10854-018-9426-0.

[32] J. Mocak, A.M. Bond, S. Mitchell, G. Scollary, A statistical overview of standard (IUPAC and ACS) and new procedures for determining the limits of detection and quantification: application to voltammetric and stripping techniques (technical report), Pure Appl. Chem. 69 (1997) 297–328, https://doi.org/10.1351/pac199769020297.

[33] G.D. Christian, P.K. Dasgupta, K.A. Schug, Analytical Chemistry, seventh ed., Wiley-VCH, New York, 2014.

[34] K. Chayavanich, W. Sapyen, A. Imyim, An easy-to-use platform for colorimetric determination of dextran: a potential application for the sugar industry, Spectrochim. Acta A Mol. Biomol. Spectroscopy 308 (2024) 123761, https://doi.org/10.1016/j.saa.2023.123761.

[35] Y. Li, Z. He, P. Zou, Y. Ning, X. Zhu, Determination of seventeen sugars and sugar alcohols in fruit juice samples using hydrophilic interaction liquid chromatography-tandem mass spectrometry combining response surface methodology design, Microchem. J. 193 (2023) 109136, https://doi.org/10.1016/j.microc.2023.109136.

[36] Y. Zhang, W. Zhang, J. Hou, J. He, K. Li, Y. Li, D. Xu, Determination of sugars and sugar alcohols in infant formula by high performance liquid chromatography with evaporative light-scattering detector, J. Chromatogr. B 1217 (2023) 123621, https://doi.org/10.1016/j.jchromb.2023.123621.

[37] A. Singh, A. Hazarika, L. Dutta, A. Bhuyan, M. Bhuyan, A fully handwritten-on-paper copper nanoparticle ink-based electroanalytical sweat glucose biosensor fabricated using dual-step pencil and pen approach, Anal. Chim. Acta 1227 (2022) 340257, https://doi.org/10.1016/j.aca.2022.340257.

[38] Y. Feng, B. Niu, H. Guo, Unusual rod-like Cu/$Cu_2O$@MOF(Cu) ternary nanocomposite modified electrode for electroanalytical sensors of glucose, Electrochim. Acta 530 (2025) 146416, https://doi.org/10.1016/j.electacta.2025.146416.

[39] Y.Z. Zhao, R. Malpass-Evans, M. Carta, N.B. McKeown, P.J. Fletcher, G. Kociok-Köhn, D. Lednitzky, F. Marken, Size-selective photoelectrochemical reactions in microporous environments: Clark probe investigation of Pt@g-$C_3N_4$ embedded into intrinsically microporous polymer (PIM-1), Chemelectrochem 8 (2021) 3499–3505, https://doi.org/10.1002/celc.202100732.